AIAA JOURNAL
Vol. 42, No. 11, November 2004

Flexible Flapping Airfoil Propulsion at Zero Freestream Velocity

S. Heathcote,* D. Martin,† and I. Gursul‡
University of Bath, Bath, England BA2 7AY, United Kingdom

Thrust generation for an airfoil plunging at zero freestream velocity, the case relevant to hovering birds and insects, has been studied. The objective was to investigate the effect of airfoil stiffness. Particle image velocimetry and force measurements were taken for three airfoils of relative bending stiffnesses 1:8:512 in a water tank. The deformation of the flexible airfoils produces an angle of attack that varies periodically with a phase angle with respect to the plunging motion. Amplitude and phase of this combined plunging/pitching motion play a major role in the flowfield and thrust generation. Vortex pairs or alternating vortex streets were observed depending on the amplitude and phase lag of the trailing edge. The strength of the vortices, their lateral spacing, and the time-averaged velocity of the induced jet were found to depend on the airfoil flexibility, plunge frequency, and amplitude. Direct force measurements confirmed that at high plunge frequencies the thrust coefficient of the airfoil with intermediate stiffness was greatest, although the least stiff airfoil can generate larger thrust at low frequencies. It is suggested that there is an optimum airfoil stiffness for a given plunge frequency and amplitude. The thrust/input-power ratio was found to be greater for the flexible airfoils than for the rigid airfoil.

Nomenclature

a	=	plunge amplitude
b	=	plate thickness
C_M	=	momentum flux coefficient
C_T	=	thrust coefficient
c	=	chord length
d	=	lateral spacing between vortex rows
E	=	modulus of elasticity
F	=	driving force
f	=	plunge frequency
h	=	dimensionless plunge amplitude, a/c
K	=	dimensionless thin-plate bending stiffness
k	=	thin-plate bending stiffness
M	=	momentum flux per unit span
Re	=	Reynolds number
s	=	displacement
T	=	thrust per unit span; period
t	=	time
U	=	fluid velocity
v	=	wing leading-edge velocity
x	=	streamwise distance
y	=	lateral distance
α	=	angle of attack
ε	=	efficiency
μ	=	viscosity
ν	=	kinematic viscosity, μ/ρ
ρ	=	density
ϕ	=	phase

Subscripts

LE	=	leading edge
p	=	peak value
TE	=	trailing edge
x	=	streamwise component

Received 2 October 2003; revision received 21 May 2004; accepted for publication 9 June 2004.

*Ph.D. Student, Department of Mechanical Engineering. Student Member AIAA.

†Undergraduate Student, Department of Mechanical Engineering.

‡Professor of Aerospace Engineering, Department of Mechanical Engineering. Associate Fellow AIAA.

Introduction

RECENT advances in microtechnology have created an opportunity to mount miniature surveillance equipment on small flying aircraft known as micro air vehicles (MAVs). Such microflying robots may be suitable for military missions such as reconnaissance and surveillance, as well as civilian applications such as coast watch, crop monitoring, telecommunications, news broadcasting, remote sensing, and mineral exploration. A large number of much smaller sized flying sensors is envisaged for atmospheric measurements and climate research.

Due to their small size and speed, MAVs fly at very low Reynolds numbers, which results in flow separation and poor aerodynamic performance. Nevertheless, the aerodynamic lift is not the limiting issue. The real challenge is in the area of propulsion systems. Flapping-wing flight has received considerable attention in the past few years as an alternative to propeller flight, which is inefficient at these small scales. The fact that birds, insects, and many sea creatures use flapping-wing propulsion successfully encouraged recent interest in the development of MAVs.[1] Plunging and pitching airfoils are known to produce thrust if the oscillation frequency or amplitude is large enough. The mechanism of thrust generation is related to the formation of a pair of opposite-sign vortices at the trailing edge of the wing during the oscillation cycle.

It seems to have been Knoller[2] in 1909 and Betz[3] in 1912 who first discovered that an oscillating airfoil produces thrust. Ten years later, Katzmayr's[4] wind-tunnel tests verified what is now known as the Knoller–Betz effect. These early experimental and theoretical investigations were summarized by Koochesfahani,[5] Jones et al.[6] and Lai and Platzer.[7] Theoretical investigations based on inviscid flow analysis established that the theoretical propulsive efficiency of a flapping airfoil could be very high. Viscous simulations of thrust generation in the absence of large-scale flow separation agreed well with the potential flow analysis.[8] However, when flow separation occurs at low Reynolds numbers, the propulsive efficiency is rapidly degraded.[9,10] Likewise, adverse effects of flow separation on propulsion at low Reynolds numbers have been observed for a MAV configuration.[11]

The limiting case of low-Reynolds-number aerodynamics is the thrust generation at zero freestream velocity.[12] This particular case is relevant to the thrust generation by many insects and birds hovering in still air. It was shown that a sharp trailing edge is required for effective thrust generation.[12] More complicated models of hovering, which involve coupled pitching and plunging motions, were studied by Freymuth[13] and Sunada et al.[14] Present work focuses on thrust generation for plunging rigid and flexible airfoils.

Since Knoller and Betz sparked interest in the subject, there have been many experimental and numerical studies of thrust coefficient

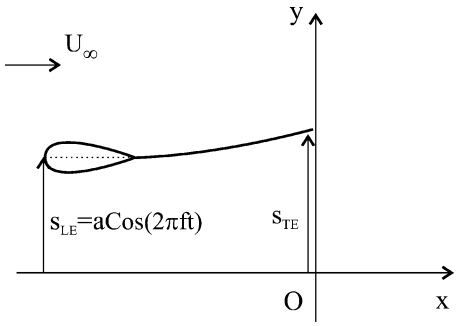

Fig. 1 Schematic of a flexible airfoil plunging periodically in the vertical direction.

and propulsive efficiency as a function of the amplitude and frequency of motion, coupled pitching and plunging motions, and airfoil shapes. Flexibility, though, has received less attention. The importance of wing flexibility remains unclear in unsteady flow of insect flight.[15] A computational study[16] of a flexible oscillating thin airfoil in inviscid flow was carried out and it was shown that flexible foils may have better efficiency. There is a suggestion that flexibility is essential for fish agility.[17] There is also growing evidence that wing flexibility may be exploited for better performance for low-Reynolds-number flows.[18]

The aim of this paper is to study the effect of flexibility by measurements of the deformation of a flexible airfoil, resulting velocity field, thrust, and ratio of thrust to input power. Comparison over a range of plunging frequencies, amplitudes, and airfoil flexibilities is made. A flexible airfoil is shown in Fig. 1. The leading edge is plunged sinusoidally with plunge amplitude a and frequency f. The displacement of the leading edge is denoted by $S_{\mathrm{LE}}(t)$ and the displacement of the trailing edge is denoted by $S_{\mathrm{TE}}(t)$. The experiments described in this paper are carried out at zero freestream velocity. Three dimensionless parameters are appropriate:

$$h = a/c, \qquad Re = fc^2/\nu, \qquad K = k/\mu\nu c$$

where $k = Eb^3/12$. Hence, h is proportional to the plunge amplitude, Re to the plunge frequency, and K to the bending stiffness of the plate k. Note that there is no freestream velocity, and therefore the Reynolds number in this case depends on the frequency and has been used in previous investigations.[13,14]

Experimental Setup

The cross section of the airfoil/plate combination tested is shown in Fig. 2. Previous work suggests that leading-edge shape has only a minor effect.[11] The airfoil has a thin flat plate of length 60 mm attached to a 30-mm-chord, 10-mm-thick airfoil. It has an overall chord length of 90 mm and span of 300 mm. The thick airfoil forming the leading edge was manufactured from solid aluminum. The plate is sheet steel with uniform thickness. The flexibility of the airfoil is varied by using plates of different thickness. Three plates, of thicknesses 0.05, 0.1, and 0.4 mm, are tested. Because the bending stiffness of a plate varies with the cube of the plate's thickness, the bending stiffnesses are in the ratio $k_1{:}k_2{:}k_3 = 0.05^3{:}0.1^3{:}0.4^3 = 1{:}8{:}512$. The three airfoils are referred to as "very flexible," "flexible," and "rigid," respectively.

Experiments are carried out in a $1.2 \times 0.5 \times 0.5$ m glass water tank (Fig. 3). The airfoil is mounted vertically and one end is attached to a horizontal shaker (Motovario 0.37-kW three-phase motor and IMO Jaguar controller). Tests are carried out for frequencies in the range of 1–2.5 Hz and amplitudes in the range of 5–25 mm. A position sensor on the motor emits one pulse for every degree of rotation, and an extra pulse every 360 deg, allowing phase information of the airfoil motion. There is a 2-mm gap between the top of the airfoil and a perspex splitter plate and a 2-mm gap between the bottom of the airfoil and the glass of the tank.

A laser sheet is used for visualization of plate deformation, which is generated from a Coherent 12-W Ar-ion continuous laser beam by cylindrical and spherical lenses. A 50-frames-per-second digital videocamera mounted underneath the tank is used to record

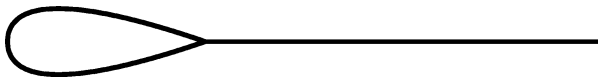

Fig. 2 Cross section of the airfoil/plate combination tested.

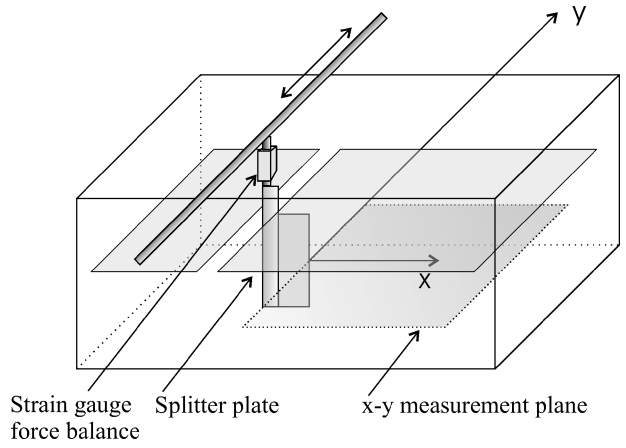

a)

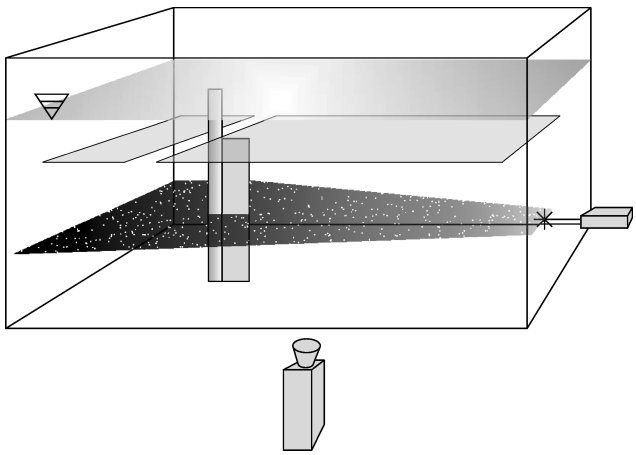

b)

Fig. 3 Experimental setup: a) overview and b) arrangement of the laser and camera for PIV measurements.

the motion of the wing. The laser sheet illuminates the x–y plane that intersects the midspan of the wing, as illustrated in Fig. 3. In the particle image velocimetry (PIV) experiments a TSI PIV system is used to measure the instantaneous velocity field in a region downstream of the trailing edge. The time between pulses from a dual YAG laser is 500 μs. The light reflects off 4-μm particles into a 2048×2048 pixel, 8-bit grayscale digital camera. The interrogation window size is 64×64 pixels with 50% overlapping. Velocity fields at a maximum rate of 3.75 Hz are recorded. A fast Fourier transform algorithm is used to determine the velocity field. An estimate of the time-averaged velocity is obtained by averaging 200 velocity fields. Ensemble averaging was used to obtain statistical information such as maximum streamwise velocity, circulation, and vortex spacing. The standard deviation of these quantities was less than 8%.

The momentum flux per unit span one chord length downstream of the trailing edge is calculated from the instantaneous velocity fields as

$$M = \rho \int \overline{U_x^2}\,\mathrm{d}y \tag{1}$$

where U_x is the instantaneous velocity and overbar denotes time averaging. A momentum flux coefficient may be defined as

$$C_M = M \Big/ \tfrac{1}{2}\rho v_p^2 c \tag{2}$$

The uncertainty of the momentum flux coefficient was estimated to be less than 10%.

A binocular strain-gauge force balance,[19] machined from aluminum, is used to make direct force measurements. Strain gauges with different sensitivities are constructed so that measurements may be taken over a wide range of plunge frequencies and amplitudes. The position of the strain gauge is shown in Fig. 3. Inertial forces were subtracted from the total force measured in any direction. The inertial forces were determined by oscillating the airfoil in air, where the fluid-dynamic forces are three orders of magnitude smaller than those generated in water. Also, the time-averaging process eliminates any contribution from the inertial forces, which have zero averages. The thrust and driving force were measured separately by rotating the strain-gauge balance. The measurement uncertainty for force coefficients was estimated as 5%. The strain-gauge signals and the motor encoder signal are sampled with a sampling rate of 100 Hz to yield a force–displacement relationship. Since $U_\infty = 0$, the thrust coefficient is defined based on the peak plunge velocity:

$$C_T = \bar{T} \Big/ \tfrac{1}{2}\rho v_p^2 c \tag{3}$$

where $v_p = 2\pi af$.

The conventional definition of propulsive efficiency cannot be used in this case, because the freestream velocity is zero. In other words, the propulsive efficiency is zero at zero freestream velocity. An alternative measure of performance is the thrust-to-power-input ratio[19]:

$$\varepsilon = \bar{T}/Fv \tag{4}$$

which has units of newton/watt and is evaluated using direct thrust and driving force measurements. The measurement uncertainty for this quantity is estimated as 8%.

Results

Flow/Structure Interaction

Figure 4 shows the very flexible plate over one oscillation cycle for $Re = 2.025 \times 10^4$ and $h = 0.194$. The inset shows the variation of location of the leading edge as a function of time. The rigid airfoil that forms the leading-edge element is partly visible. The deformation of the airfoil shown in Fig. 4 produces an angle of attack as well as a camber, which varies periodically with phase

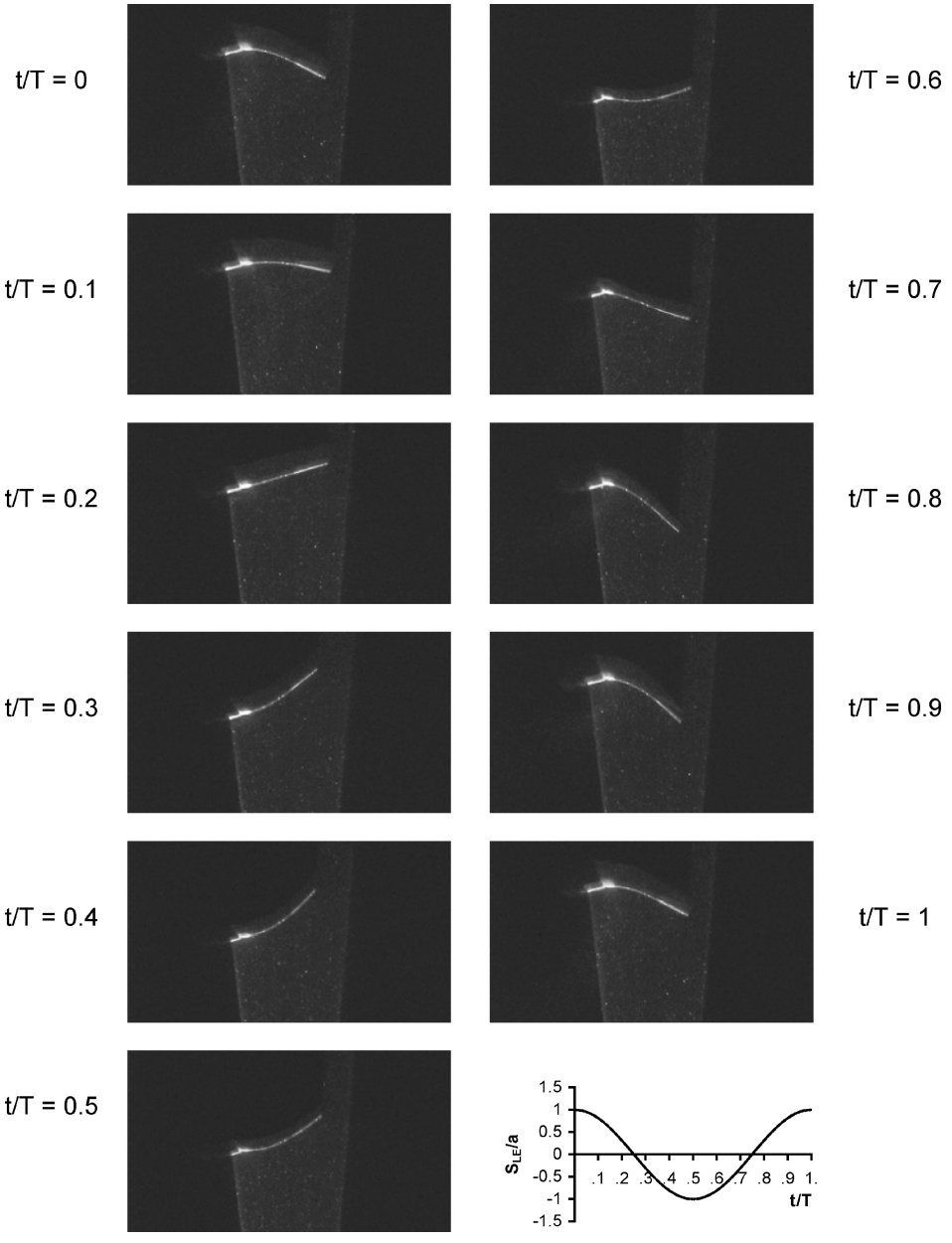

Fig. 4 Shape of the very flexible airfoil over one period ($Re = 2.025 \times 10^4$; $h = 0.194$).

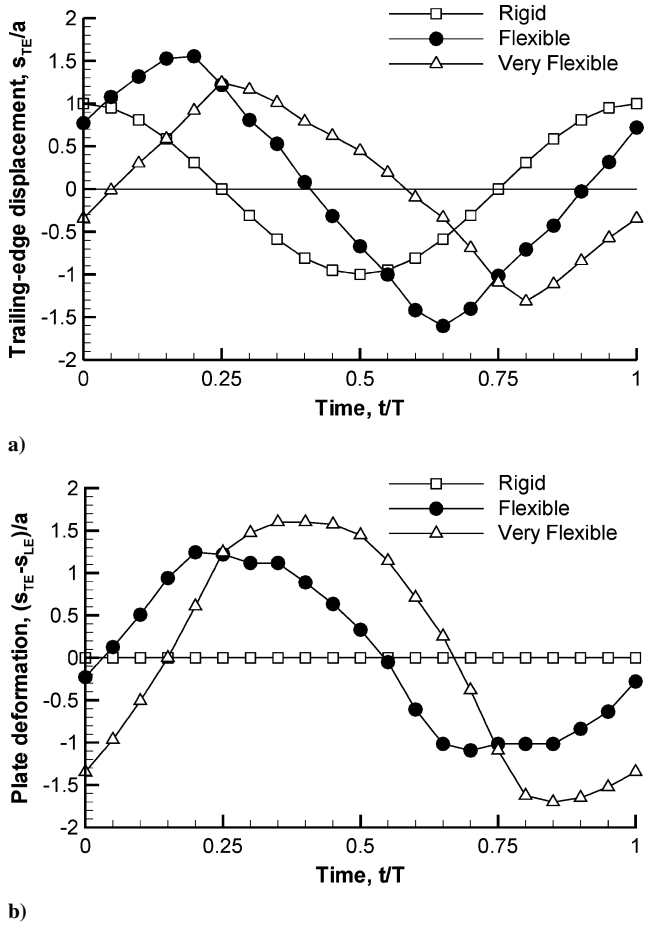

Fig. 5 Displacement of a) the trailing edge and b) the trailing edge relative to the leading edge ($Re = 2.025 \times 10^4$; $h = 0.194$).

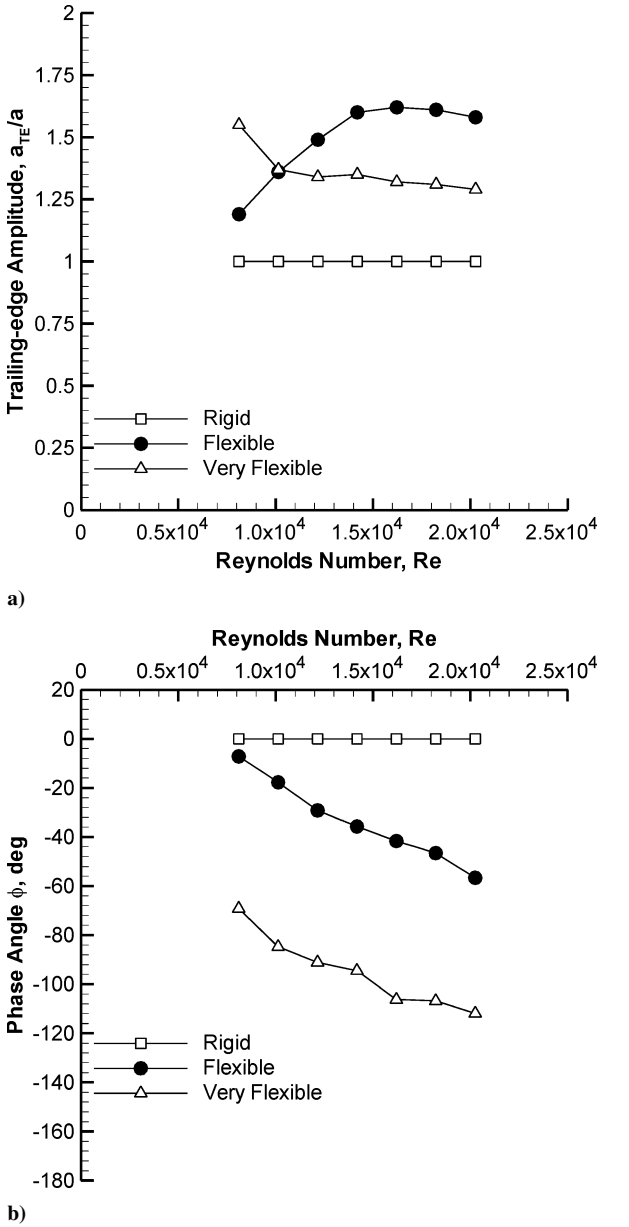

Fig. 6 S_{TE}/a as a function of Reynolds number ($h = 0.194$): a) amplitude and b) phase.

angle with respect to plunging motion. For the rigid airfoil, the pure plunging motion at zero freestream velocity produces effective angles of attack of +90 or −90 deg. However, for a flexible airfoil, pitching angle is generally negative during the downward plunging motion, which results in an effective angle of attack smaller than 90 deg. This pitching motion appears to play a major role in the flowfield and thrust production, as will be discussed.

The instantaneous location of the trailing edge of the plate was measured and is plotted in Fig. 5a. The variation of location of the trailing edge for the other airfoils is shown in the same figure. It is seen that the displacement of the trailing edge has a large phase lag for the flexible wings. Surprisingly, the maximum values of the displacement are smaller for the very flexible plate than for the flexible plate. This is due to the phase lag between the plunging motion and deformation of the flexible plates. Figure 5b shows the displacement of the trailing edge relative to the leading edge, which is the time history of the relative deformation. It is seen that the deformation of the very flexible plate is larger and the phase lag is also substantial. Nevertheless, the amplitude of the deformation is not very different for the two cases. The phase delay, however, appears to play a major role, as will be discussed.

Because the deformation and dynamic response of the flexible plates affect the resulting flow considerably, the response of the plates will be summarized in this section before the results of the velocity and force measurements are presented. Because the first bending mode is dominant in the range of the parameters tested, the amplitude and phase angle of the trailing edge are sufficient to characterize the dynamic response of the plates. Figure 6 shows the variation of amplitude and phase of displacement of the trailing edge as a function of Reynolds number for $h = 0.194$. The trailing-edge amplitude is greater than the leading-edge amplitude for both the flexible and very flexible airfoils over the range of frequencies tested. The trailing-edge amplitude of the flexible plate first increases and then decreases with frequency. The trailing-edge amplitude of the very flexible plate decreases steadily with frequency and the curves cross at around $Re = 1.0 \times 10^4$. For higher Reynolds numbers, the amplitude of the motion of the trailing edge is larger for the flexible plate than for the very flexible plate as a consequence of combined plunging motion and dynamic deformation.

Note that the displacement of the trailing edge depends on the amplitude and phase angle of deformation with respect to the plunging motion. This variable is different from that for the deformation only. If the deformation only is considered, it increases with Reynolds number as shown in Ref. 20. It is seen from Fig. 6b that the phase lag increases roughly linearly with frequency for the two flexible plates. The phase lag is approximately 60 deg greater for the very flexible airfoil. Figure 7 shows the amplitude and phase of the trailing edge as a function of plunge amplitude for $Re = 1.62 \times 10^4$. Once again, the trailing-edge amplitude is greater than the leading-edge amplitude for both the flexible and very flexible airfoils over the range of frequencies tested. The normalized trailing-edge amplitude decreases with increasing plunge amplitude for both the flexible and very flexible airfoils. The phase lag is almost independent of plunge frequency but depends greatly on the flexibility of the airfoil.

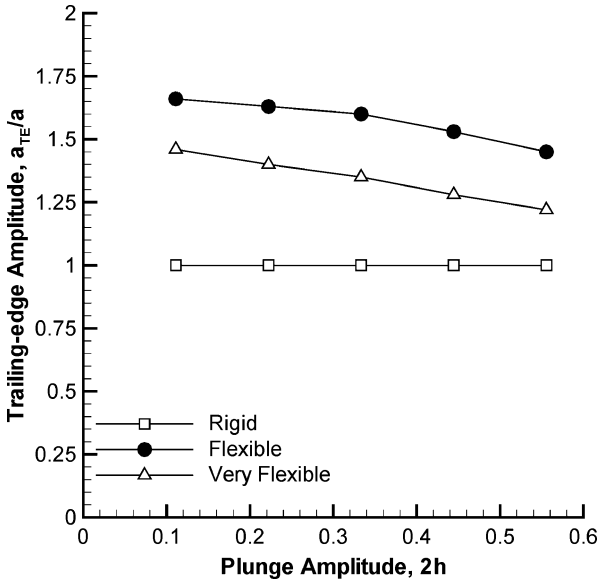

a)

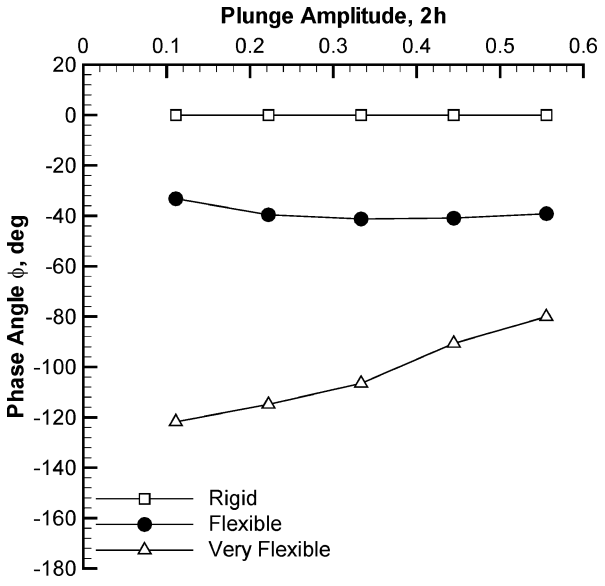

b)

Fig. 7 S_{TE}/a as a function of plunge amplitude ($Re = 1.62 \times 10^4$): a) amplitude and b) phase.

Velocity Measurements

Figure 8 shows the instantaneous velocity fields for the three plates, corresponding to Fig. 5 ($Re = 2.025 \times 10^4$; $h = 0.194$). It is seen that the structure of the vortical flow is similar for the rigid and flexible plates, resembling vortex pairs released periodically. Three differences are observed: the vortices from the flexible airfoil are slightly stronger, slightly farther apart in the lateral direction, and appear to be preserved farther downstream than the vortices from the rigid airfoil. A quite different flow structure resembling a reverse von Kármán vortex street is observed for the very flexible plate. The vortices are weaker and closer in the lateral direction; much lower induced velocities are observed.

Over a wide range of frequencies and amplitudes of plunging motion tested, it was found that the instantaneous flow structures were similar to those shown in Fig. 8: vortex pairs for the rigid and flexible plates, and alternating vortex street for the very flexible plate. It is shown in Ref. 20 that the corresponding time-averaged velocity field for all three plates is nearly parallel and symmetric. Again, higher velocities are observed for the flexible plate compared to the other two plates.

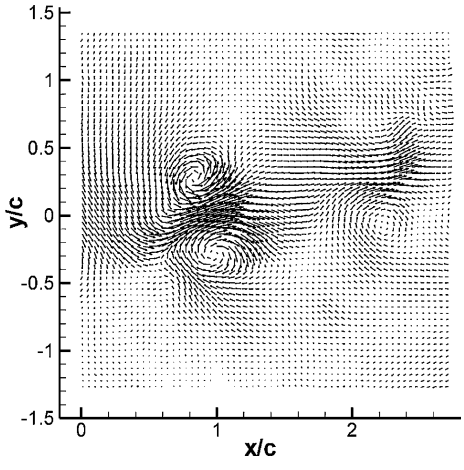

a)

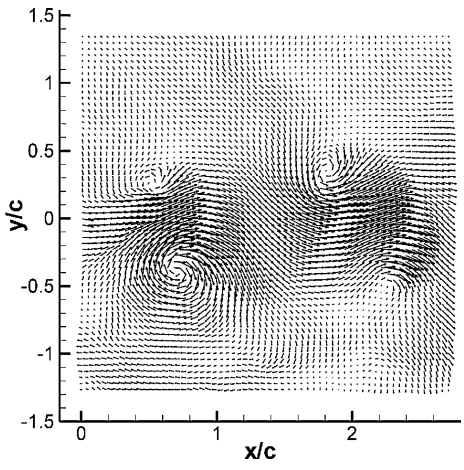

b)

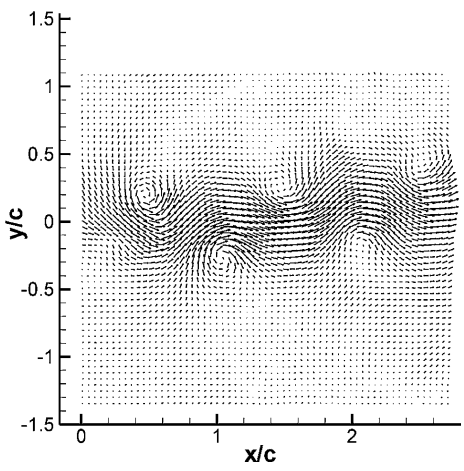

c)

Fig. 8 Instantaneous velocity field for a) the rigid airfoil, b) the flexible airfoil, and c) the very flexible airfoil ($Re = 2.025 \times 10^4$; $h = 0.194$).

Instantaneous and time-averaged flowfields were studied in detail for further statistical information. The strength of the vortices generated close to the oscillating plate was calculated as a line integral of velocity around a square path that is centered on the vortex core and covers the whole vortex, for each instantaneous flowfield. The average circulation of the vortices is shown in Fig. 9 as a function of Reynolds number. The strength is slightly larger for the flexible plate than for the rigid one, but there are substantial differences from the very flexible plate at high Reynolds numbers. The vortex strength is almost constant for the rigid and flexible airfoils but decreases rapidly with increasing Reynolds number for the very flexible plate.

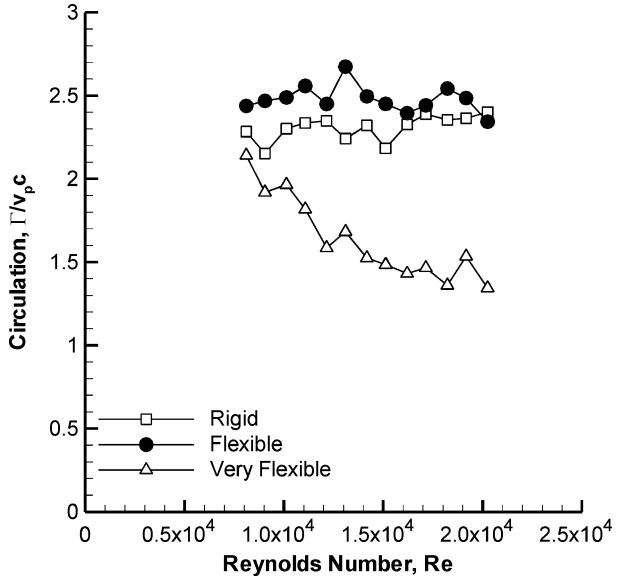

Fig. 9 Variation of normalized circulation as a function of Reynolds number ($h = 0.194$).

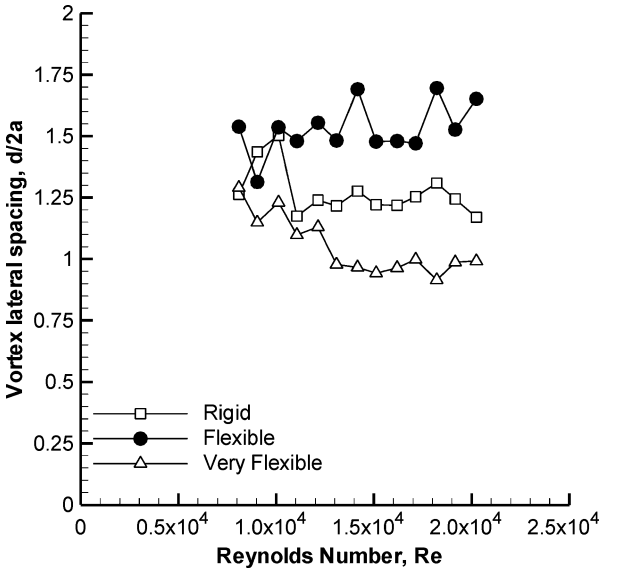

Fig. 11 Variation of normalized lateral vortex spacing as a function of Reynolds number ($h = 0.194$).

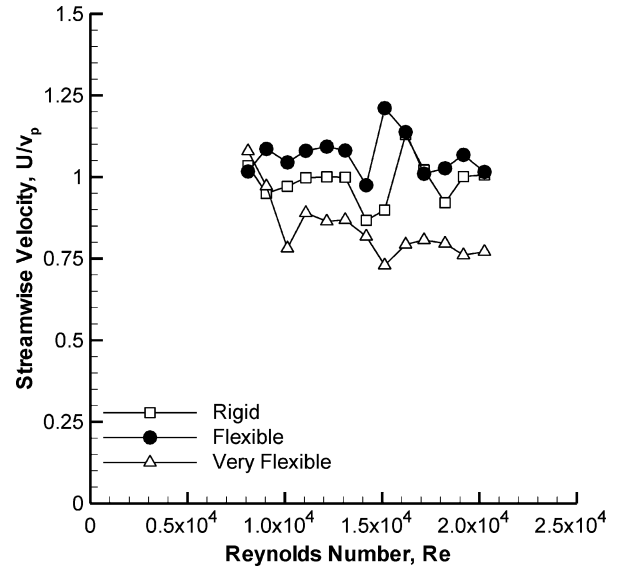

Fig. 10 Variation of maximum time-averaged streamwise velocity as a function of Reynolds number ($h = 0.194$, $x/c = 1$).

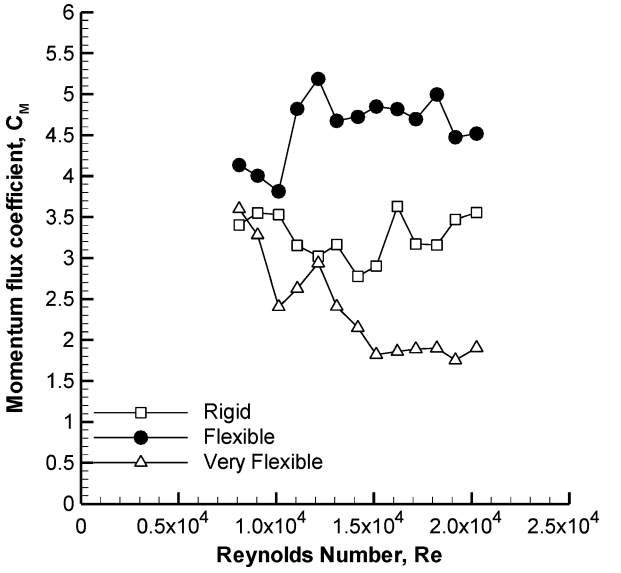

Fig. 12 Momentum flux coefficient as a function of Reynolds number ($h = 0.194$).

The variation of the maximum time-averaged jet velocity is shown in Fig. 10. The variation of streamwise velocity with Reynolds number is seen to be similar to the variation of circulation with Reynolds number, although the flexibility of the plates seems slightly less important. The maximum time-averaged velocity is roughly equal to the peak plunge velocity. Figure 11 shows the lateral spacing of the vortex rows as a function of Reynolds number. The plate stiffness is seen to have a profound effect on the separation of the vortices, a quantity roughly proportional to the mass flux of the induced jet. The largest spacing is observed for the flexible plate, whereas the smallest spacing (roughly equal to the peak-to-peak plunge amplitude) is observed for the very flexible plate. The effect of the flexibility is more important at higher Reynolds numbers.

From the instantaneous velocity information the momentum flux was calculated, which is related to the generated thrust and was used in previous investigations[5] to estimate it. However, this control-volume approach has its limitations due to large fluctuations in velocity and deviation of pressure from the freestream value at the downstream measurement station.[10] In addition, for the case of $U_\infty = 0$, there is some momentum flux across the boundary upstream of the oscillating wing. Nevertheless, the momentum flux downstream provides useful information about the flowfield generated by a plunging airfoil. In Fig. 12, the variation of momentum flux with Reynolds number is shown for each plate. The momentum flux is greatest for the flexible plate and smallest for the very flexible plate. This implies that there is an optimum flexibility. The variation of the momentum flux resembles that of the vortex lateral spacing, indicating that the most important contribution comes from the effective jet width and mass flux.

Figures 13–16 show the variation of circulation, peak time-averaged velocity, vortex spacing, and momentum flux with plunge amplitude for $Re = 1.62 \times 10^4$. Figure 13 shows that the strength of the vortices is the smallest for the very flexible plate. There is a rapid decrease of the normalized circulation with increasing plunge amplitude for the two flexible airfoils. The variation of the maximum time-averaged jet velocity normalized by the peak plunge velocity is shown in Fig. 14. The maximum time-averaged velocity decreases rapidly with increasing plunge amplitude for all three airfoils. The effect of plunge amplitude on the average lateral separation of the vortex rows is shown in Fig. 15. At small amplitudes, the vortex

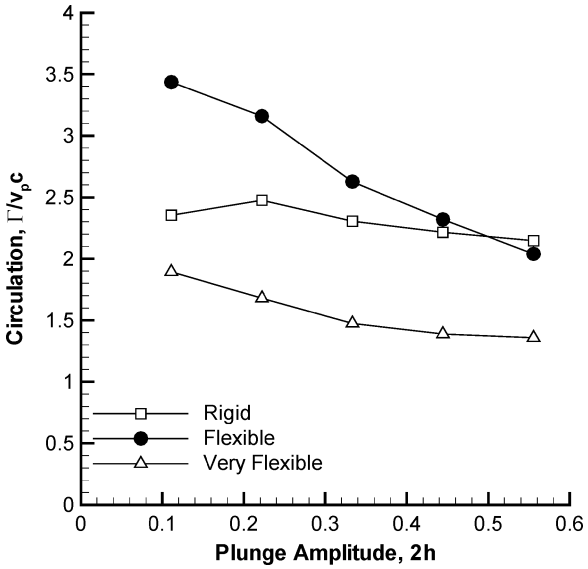

Fig. 13 Variation of normalized circulation as a function of plunge amplitude ($Re = 1.62 \times 10^4$).

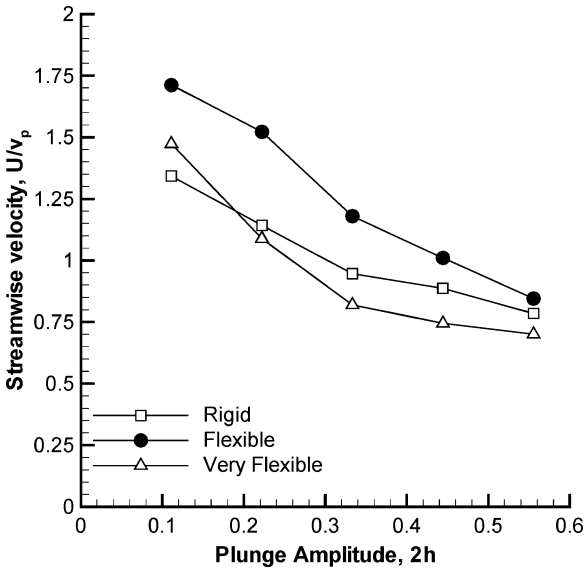

Fig. 14 Variation of maximum time-averaged streamwise velocity as a function of plunge amplitude ($Re = 1.62 \times 10^4$; $x/c = 1$).

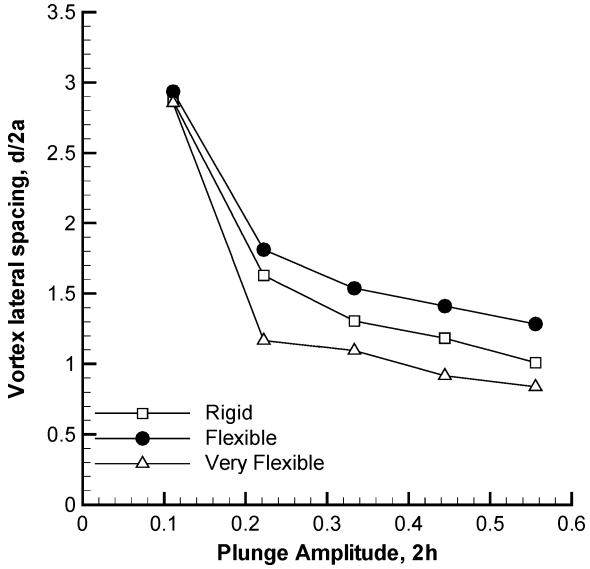

Fig. 15 Variation of normalized lateral vortex spacing as a function of plunge amplitude ($Re = 1.62 \times 10^4$).

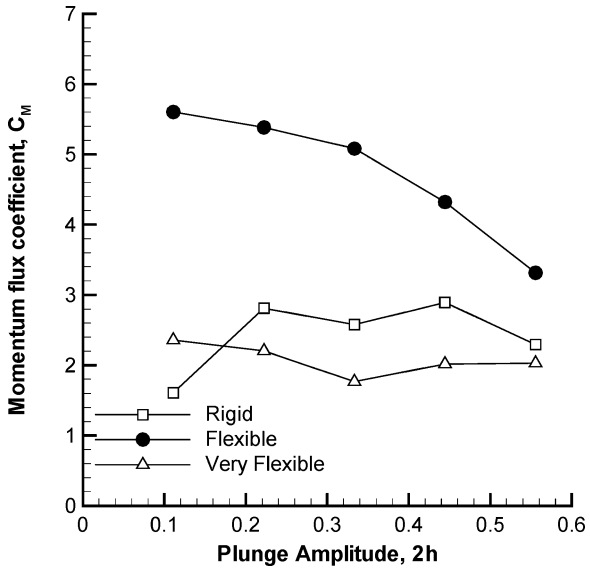

Fig. 16 Momentum flux coefficient as a function of amplitude ($Re = 1.62 \times 10^4$).

spacing is as high as three times the peak-to-peak plunge amplitude. At high amplitudes, the normalized vortex spacing approaches unity. Note that there is a similarity between the variations of the vortex lateral spacing and the time-averaged jet velocity (Fig. 14).

The variation of the momentum flux as a function of plunge amplitude is shown in Fig. 16. For comparison, Ref. 12 reports velocity measurements for pure plunging motion of a NACA 0012 airfoil. The momentum flux was estimated from the velocity measurements in Ref. 12. The momentum flux coefficients of $C_M = 1.6$ and 2.24 were found for $2h = 0.08$ and 0.494, respectively. These estimated values are in good agreement with the results shown in Fig. 16, in spite of the differences in geometry of the rigid airfoils and Reynolds numbers. It is seen in Fig. 16 that at small amplitudes the momentum flux is a factor of 2 to 3 greater for the flexible plate than for the very flexible or rigid plates. At higher amplitudes the three curves converge; the effect of flexibility appears to be diminished. Although the flexible plate provides the largest momentum flux at small plunge amplitudes, it decreases rapidly with increasing amplitude. The results shown in Figs. 9–16 suggest that the flexible plate generates larger thrust in general. These results were studied more closely by direct force measurements.

Force Measurements

Figure 17 shows the variation of the thrust coefficient obtained directly from force measurements as a function of Reynolds number for $h = 0.194$. For $Re < 1.0 \times 10^4$, the very flexible plate has the greatest thrust coefficient. It falls rapidly though, and for $Re > 1.0 \times 10^4$ the flexible plate has the greatest thrust coefficient. The thrust coefficient for the rigid plate increases almost linearly with Reynolds number. With the exception of the rigid plate, the trends in the momentum flux coefficient and thrust coefficient are similar. The magnitudes of the momentum flux and thrust coefficients differ by a factor of roughly 2, illustrating that downstream momentum flux is not sufficient for an accurate estimate of the thrust. Figure 18 shows the variation of the thrust coefficient obtained directly from force measurements as a function of plunge amplitude for $Re = 1.62 \times 10^4$. There is again a similar trend with the momentum flux coefficient obtained from PIV measurements. For coupled pitching and plunging studies reported in Refs. 13 and 14, the momentum flux and force coefficients (relatively high thrust coefficients in the range of 1–3) for typical pitching amplitudes corresponding to our case are consistent with the data for zero freestream velocity.

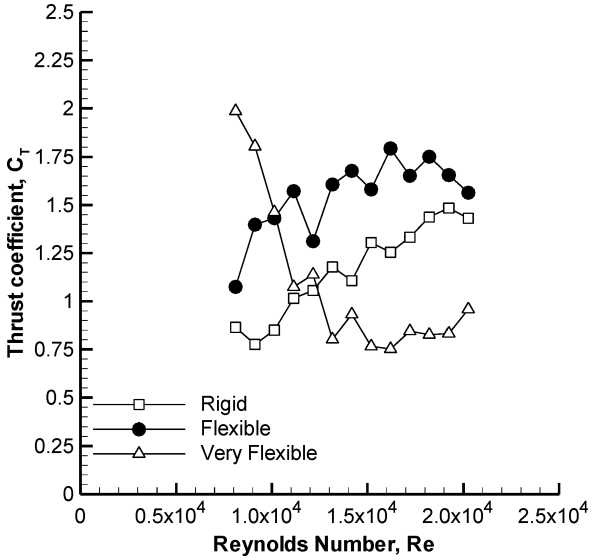

Fig. 17 Variation of thrust coefficient with Reynolds number ($h = 0.194$).

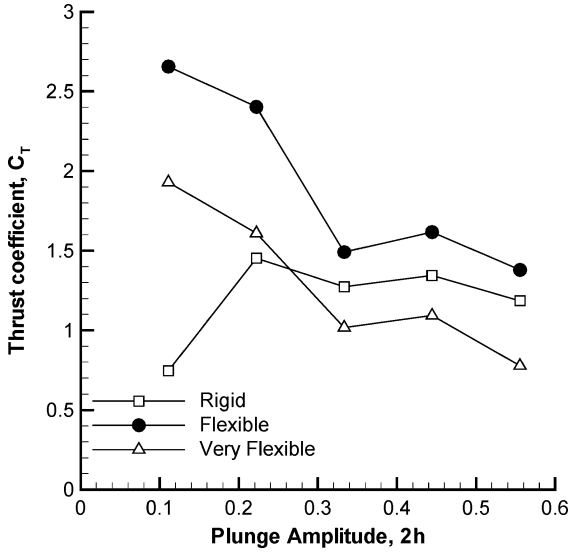

Fig. 18 Variation of thrust coefficient with plunge amplitude ($Re = 1.62 \times 10^4$).

In Figs. 19a and 19b, the variation of thrust per unit power input with Reynolds number and plunge amplitude is shown. The power input is calculated from the strain-gauge measurements of driving force and the velocity of the airfoil. The very flexible plate is seen to be the most efficient for all values of Reynolds number and the rigid plate the least. This behavior is qualitatively different from the variation of thrust with Reynolds number, where the flexible plate provides larger thrust, except at very low Reynolds numbers. The efficiency of the very flexible plate is particularly high at low Reynolds numbers but, as with the thrust coefficient (Fig. 17), it falls rapidly. The efficiency of the flexible plate declines gradually with increasing Reynolds number. The efficiency of the rigid plate is remarkably constant. In Fig. 19b, thrust per unit power input is plotted as a function of plunge amplitude. Over the range of plunge amplitudes tested the very flexible plate is the most efficient and the rigid plate the least. The general trend is for the efficiency to fall with plunge amplitude.

Conclusions

Thrust generation for an airfoil plunging at zero freestream velocity, the case relevant to insects and birds moving off from rest, was studied. The objective was to study the effect of airfoil stiffness. PIV and force measurements were taken for three airfoils of relative bending stiffness 1:8:512.

The displacement of the trailing edge of flexible airfoils was found to be larger than that of the rigid airfoil and also to lag the displacement of the leading edge. The maximum values of the instantaneous displacement are generally smaller for the very flexible airfoil than for the flexible airfoil as a consequence of large phase lags between the deformation and plunging motion. This phase lag, which increased with wing flexibility and plunge frequency, produced very different vortical flows. Vortex pairs for the rigid and flexible plates, and alternating vortex streets for the very flexible plate, were observed. The angle of attack and camber of the flexible airfoil determines the velocity outside the boundary layer at the separation point (trailing edge). Because the trailing edge is a major source of shedding of vorticity at zero freestream velocity, the amplitude and phase angle of the motion of the trailing edge affect the strength and spacing of the vortices.

The strength of vortices is slightly larger for the flexible plate than for the rigid one, but there are substantial differences from the very flexible plate, in particular at high Reynolds numbers. The airfoil flexibility has a much more pronounced effect on the vortex spacing, which is roughly proportional to the mass flux of the induced jet. The largest spacing is observed for the flexible plate, whereas the smallest spacing is observed for the very flexible plate. The calculated momentum flux is greatest for the flexible plate, but the very flexible

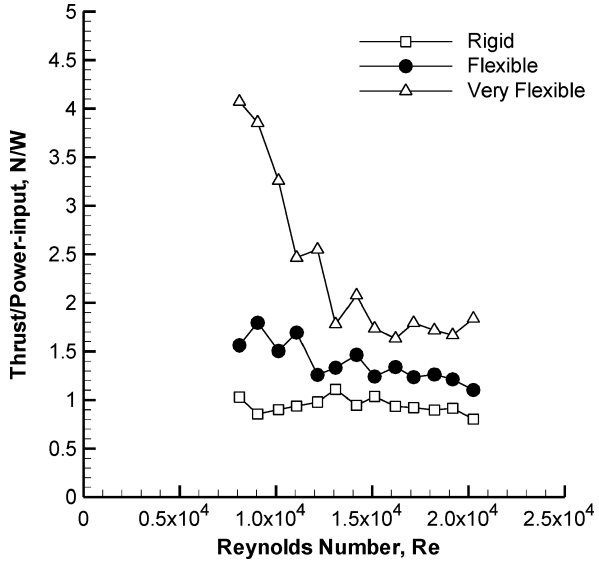

a)

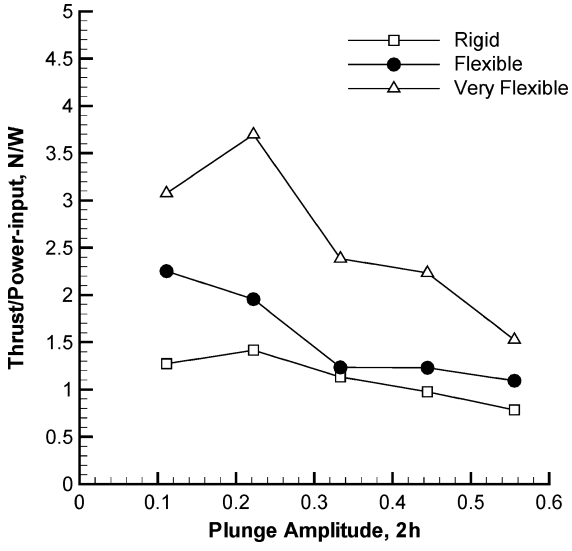

b)

Fig. 19 Thrust/power ratio as a function of a) Reynolds number ($h = 0.194$) and b) amplitude ($Re = 1.62 \times 10^4$).

plate performs even worse than the rigid plate, implying that there is an optimum flexibility. There is a strong effect of plunge amplitude on the circulation of vortices, time-averaged velocity, and vortex spacing. The calculated momentum flux indicates large influence of flexibility at small amplitudes.

Direct force measurements confirmed that at high plunge frequencies the thrust coefficient of the airfoil with intermediate stiffness was greatest, although the least stiff airfoil can generate larger thrust at low frequencies. No regime was found in which the stiffest, essentially rigid, airfoil performed best. It is suggested that there is an optimum airfoil stiffness that maximizes thrust for a given plunge frequency and amplitude. The thrust/input-power ratio was found to be greater for the flexible airfoils than for the rigid airfoil.

Acknowledgment

This work has been supported by an Engineering and Physical Sciences Research Council studentship.

References

[1]Spedding, G. R., and Lissaman, P. B. S., "Technical Aspects of Microscale Flight Systems," *Journal of Avian Biology*, Vol. 29, No. 4, 1998, pp. 458–468.

[2]Knoller, R., "Die Gesetze des Luftwiderstandes," *Flug- und Motortechnik (Wien)*, Vol. 3, No. 21, 1909, pp. 1–7.

[3]Betz, A., "Ein Beitrag zur Erklaerung des Segelfluges," *Zeitschrift fuer Flugtechnik und Motorluftschiffahrt*, Vol. 3, No. 21, 1912, pp. 269–272.

[4]Katzmayr, R., "Effect of Periodic Changes of Angle of Attack on Behaviour of Airfoils," NACA Rept. 147, Oct. 1922.

[5]Koochesfahani, M. M., "Vortical Patterns in the Wake of an Oscillating Airfoil," *AIAA Journal*, Vol. 27, No. 9, 1989, pp. 1200–1205.

[6]Jones, K. D., Dohring, C. M., and Platzer, M. F., "Experimental and Computational Investigation of the Knoller–Betz Effect," *AIAA Journal*, Vol. 36, No. 7, 1998, pp. 1240–1246.

[7]Lai, J. C. S., and Platzer, M. F., "Jet Characteristics of a Plunging Airfoil," *AIAA Journal*, Vol. 37, No. 12, 1999, pp. 1529–1537.

[8]Tuncer, I. H., and Platzer, M. F., "Thrust Generation Due to Airfoil Flapping," *AIAA Journal*, Vol. 34, No. 2, 1996, pp. 324–331.

[9]Isogai, K., Shinmoto, Y., and Watanabe, Y., "Effects of Dynamic Stall on Propulsive Efficiency and Thrust of Flapping Airfoil," *AIAA Journal*, Vol. 37, No. 10, 1999, pp. 1145–1151.

[10]Ramamurti, R., and Sandberg, W., "Simulation of Flow About Flapping Airfoils Using Finite Element Incompressible Flow Solver," *AIAA Journal*, Vol. 39, No. 2, 2001, pp. 253–260.

[11]Jones, K. D., and Platzer, M. F., "Flapping Wing Propulsion for a Micro Air Vehicle," AIAA Paper 2000-0897, Jan. 2000.

[12]Lai, J. C. S., and Platzer, M. F., "Characteristics of a Plunging Airfoil at Zero Freestream Velocity," *AIAA Journal*, Vol. 39, No. 3, 2001, pp. 531–534.

[13]Freymuth, P., "Thrust Generation by an Airfoil in Hover Modes," *Experiments in Fluids*, Vol. 9, No. 1, 1990, pp. 17–24.

[14]Sunada, S., Kawachi, K., Matsumoto, A., and Sakaguchi, A., "Unsteady Forces on a Two-Dimensional Wing in Plunging and Pitching Motions," *AIAA Journal*, Vol. 39, No. 7, 2001, pp. 1230–1239.

[15]Maxworthy, T., "The Fluid Dynamics of Insect Flight," *Annual Review of Fluid Mechanics*, Vol. 13, 1981, pp. 329–350.

[16]Murray, M. M., "Hydroelasticity Modeling of Flexible Propulsors," Ph.D. Dissertation, Dept. of Mechanical Engineering and Materials Science, Duke Univ., Durham, NC, 2000; also Murray, M. M., and Howle, L. E., "Spring Stiffness Influence on an Oscillating Propulsor," *Journal of Fluids and Structures*, Vol. 17, No. 7, 2003, pp. 915–926.

[17]Triantafyllou, M. S., Triantafyllou, G. S., and Yue, D. K. P., "Hydrodynamics of Fishlike Swimming," *Annual Review of Fluid Mechanics*, Vol. 32, 2000, pp. 33–53.

[18]Shyy, W., Berg, M., and Ljungqvist, D., "Flapping and Flexible Wings for Biological and Micro Air Vehicles," *Progress in Aerospace Sciences*, Vol. 35, No. 5, 1999, pp. 455–505.

[19]Frampton, K. D., Goldfarb, M., Monopoli, D., and Cveticanin, D., "Passive Aeroelastic Tailoring for Optimal Flapping Wings," *Fixed and Flapping Wing Aerodynamics for Micro Air Vehicle Applications*, edited by T. J. Mueller, Vol. 185, Progress in Astronautics and Aeronautics, AIAA, Reston, VA, 2001.

[20]Heathcote, S., Martin, D., and Gursul, I., "Flexible Flapping Wing Propulsion at Zero Freestream Velocity," AIAA Paper 2003-3446, June 2003.

H. Reed
Associate Editor